

RESEARCH ARTICLE

10.1029/2018JE005532

Special Section:

Science and Exploration of the Moon, Near-Earth Asteroids, and the Moons of Mars

Key Points:

- We combined the superposition T-matrix and static structure factor correction methods
- Our method captured scattering by densely packed particles in elementary volumes of radiative transfer
- We improved the modeling of spectral features arising from volume scattering

Correspondence to:

G. Ito,
gen.ito@stonybrook.edu

Citation:

Ito, G., Mishchenko, M. I., & Glotch, T. D. (2018). Radiative-transfer modeling of spectra of planetary regoliths using cluster-based dense packing modifications. *Journal of Geophysical Research: Planets*, 123, 1203–1220. <https://doi.org/10.1029/2018JE005532>

Received 11 JAN 2018

Accepted 30 MAR 2018

Accepted article online 19 APR 2018

Published online 20 MAY 2018

Radiative-Transfer Modeling of Spectra of Planetary Regoliths Using Cluster-Based Dense Packing Modifications

Gen Ito^{1,2} , Michael I. Mishchenko², and Timothy D. Glotch¹ ¹Department of Geosciences, Stony Brook University, Stony Brook, NY, USA, ²NASA Goddard Institute for Space Studies, New York, NY, USA

Abstract In remote sensing of planetary bodies, the development of analysis techniques that lead to quantitative interpretations of data sets has relatively been deficient compared to the wealth of acquired data, especially in the case of regoliths with particle sizes on the order of the probing wavelength. Radiative transfer theory has often been applied to the study of densely packed particulate media like planetary regoliths, but with difficulty; here we continue to improve theoretical modeling of spectra of densely packed particulate media. We use the superposition T-matrix method to compute the scattering properties of an elementary volume entering the radiative transfer equation by modeling it as a cluster of particles and thereby capture the near-field effects important for dense packing. Then, these scattering parameters are modified with the static structure factor correction to suppress the irrelevant far-field diffraction peak rendered by the T-matrix procedure. Using the corrected single-scattering parameters, reflectance (and emissivity) is computed via the invariant-embedding solution to the scalar radiative transfer equation. We modeled the emissivity spectrum of the 3.3 μm particle size fraction of enstatite, representing a common regolith component, in the midinfrared ($\sim 5\text{--}50 \mu\text{m}$). The use of the static structure factor correction coupled with the superposition T-matrix method produced better agreement with the corresponding laboratory spectrum than the sole use of the T-matrix method, particularly for volume scattering wavelengths (transparency features). This work demonstrates the importance of proper treatment of the packing effects when modeling semi-infinite densely packed particulate media using finite, cluster-based light scattering models.

Plain Language Summary Currently, remote sensing measurements from spacecraft and ground-based observatories are the main means to understand the characteristics of various solar system objects. Remote sensing data can be complex and difficult to interpret, yet their correct interpretation is critical in making scientific findings. Surfaces of many solar system objects are covered with regolith—soil-like material made of fine particles of ices, minerals, and rock fragments. Remote sensing data from such surfaces pose a challenge to accurate interpretations and require improved analysis techniques. Our work takes some of the initial steps in addressing this problem by capturing and modeling one of the fundamental physical processes of remote sensing, known as light scattering. We present a light scattering model that has been tailored, to a reasonable extent, to meet the conditions of planetary regoliths. Our model places particular emphasis on accurately representing the packing (how condensed) of the regolith particles. This leads to more accurate results than previous models, within limits of the scope of our method. Our method contributes to the unfolding development of ever-improving light scattering models for accurate remote sensing data analyses.

1. Introduction

Light scattering and radiative transfer models are important tools in optical characterization of particulate media and have been an integral part in analyses of atmospheres and surfaces of solar system bodies from various remote sensing measurements (e.g., of the Earth; Maignan et al., 2004; Mars; Clancy et al., 2003; Glotch et al., 2016; Poulet et al., 2008, 2009; Smith et al., 2000; Wolff & Clancy, 2003; Wolff et al., 2006, 2009; Jupiter; Dlugach, 2016; Dlugach & Mishchenko, 2005; Mishchenko, 1990; and asteroids, moons, and other small bodies; Dlugach, 2016; Hapke, 1981, 1993, 2012; Kolokolova et al., 2010, 2011; Lumme & Bowell, 1981b; Mishchenko et al., 2010; Pitman et al., 2017; Poulet et al., 2002; Shkuratov et al., 1999; Tishkovets & Petrova, 2017). In the strictest sense, the radiative transfer theory (RTT) can only be applied to

sparse particulate media in which individual particles are separated enough from each other that the far-field approximation can be assumed (Mishchenko, 2014; Mishchenko et al., 2006; van de Hulst, 1957). However, the RTT has still been applied to densely packed media, such as regoliths and snow surfaces, with a variety of assumptions and modifications (Cheng et al., 2010; Conel, 1969; Hapke, 1981, 1993, 2012; Lumme & Bowell, 1981a; Mishchenko et al., 1999; Moersch & Christensen, 1995; Muinonen et al., 2015, 2017, 2018; Mustard & Hays, 1997; Pitman et al., 2005; Reichardt & Kulp, 2016; Tishkovets & Petrova, 2013a, 2013b, 2016, 2017; Tsang, 1992; Tsang et al., 1985; Videen & Muinonen, 2015; Wald, 1994; Wald & Salisbury, 1995; Wiscombe & Warren, 1980; Xiong & Shi, 2014; Xiong et al., 2015; Zurk et al., 1996).

Simultaneous analyses of both photometric and polarimetric data are known to yield precise microphysical and macrophysical information on planetary objects (e.g., Mishchenko et al., 2010; Mishchenko & Travis, 1997). In many cases, however, solitary use of photometric data is common, and furthermore, spectra of bidirectional and hemispherically averaged reflectances and emissivities can be quite informative and have led to important contributions to the understanding of planetary bodies such as indications of water on Mars and the Moon (e.g., Christensen et al., 2001; Pieters et al., 2009). Some spectral analysis procedures in the mid-infrared wavelengths ($\sim 5\text{--}50\ \mu\text{m}$) utilize a mathematical approach for deconvolving complex mineral spectra into their constituent phases (e.g., Feely & Christensen, 1999; Pan et al., 2015; Ramsey & Christensen, 1998; Rogers & Aharonson, 2008; Thorpe et al., 2015) and are capable of bypassing the use of rigorous light scattering modeling. One limitation in this approach, however, arises when analyzing regolith surfaces with particle sizes in the “resonance” regime, where particle diameters are on the order of or smaller than the wavelength used in remote sensing measurements, leading to nonlinear spectral mixing. The resonance regime frequently occurs for a variety of solar system objects, requiring physically based models that can accommodate nonlinear traits. Our study takes a step closer toward the goal of providing a rigorous, physically based model for spectral analysis and resolving the difficulty of the resonance regime with the use of some of the most recent advances in accurate numerical procedures in light scattering and radiative transfer modeling.

Various attempts have been made to model spectra of planetary regoliths (or their proxies) with the RTT, but satisfying results, where the models can be confidently implemented in analyses of real remote sensing data, are still challenging to obtain (Conel, 1969; Ito et al., 2017; Moersch & Christensen, 1995; Mustard & Hays, 1997; Pitman et al., 2005; Wald, 1994; Wald & Salisbury, 1995). One problem is the difficulty in proper incorporation of the near-field effects important in densely packed particulate media. Tishkovets and Petrova (2013a, 2013b, 2016, 2017), Glotch et al. (2016), and Ito et al. (2017) used the “single-scattering” parameters obtained with the superposition T-matrix method as inputs into radiative transfer models to capture the near-field effects for closely packed particles in a particulate surface. This approach was a valuable improvement over the standard Mie-based models. However, one potential issue is that the T-matrix procedure by definition computes the scattering pattern in the far zone of an elementary volume of particulate medium and thereby yields a strong diffraction peak caused by the forward-scattering interference of the waves scattered by the individual particles within the elementary volume. Obviously, this expressly far-field scattering feature is irrelevant in the study of light scattering by adjacent elementary volumes. For this reason, we implement the so-called static structure factor correction to the single-scattering properties of the elementary volume obtained by the superposition T-matrix method in order to suppress this undesirable artifact.

2. Methods

2.1. Elementary-Volume Scattering Parameter Computation

Our approach in modeling the spectra of densely packed particulate media is based on the phenomenological RTT (Chandrasekhar, 1950) and as such has three major components. The first two serve to compute the single-scattering properties of an elementary volume of particulate medium serving as a centerpiece of the conceptual foundation of the RTT (Figure 1). The third one is the computer solution of the RTT formulated for a semi-infinite layer of regolith.

First, the single-scattering parameters of an elementary volume are initially computed using the superposition T-matrix method (Dlugach et al., 2011; Mackowski, 1994; Mackowski & Mishchenko, 1996, 2011). Specifically, the elementary volume is assumed, for simplicity, to be a small spherical volume of space populated by a number of densely packed, randomly positioned particles (cf. Tishkovets & Petrova, 2013a, 2016, 2017). As such, the elementary volume can also be viewed as a random cluster of closely spaced particles.

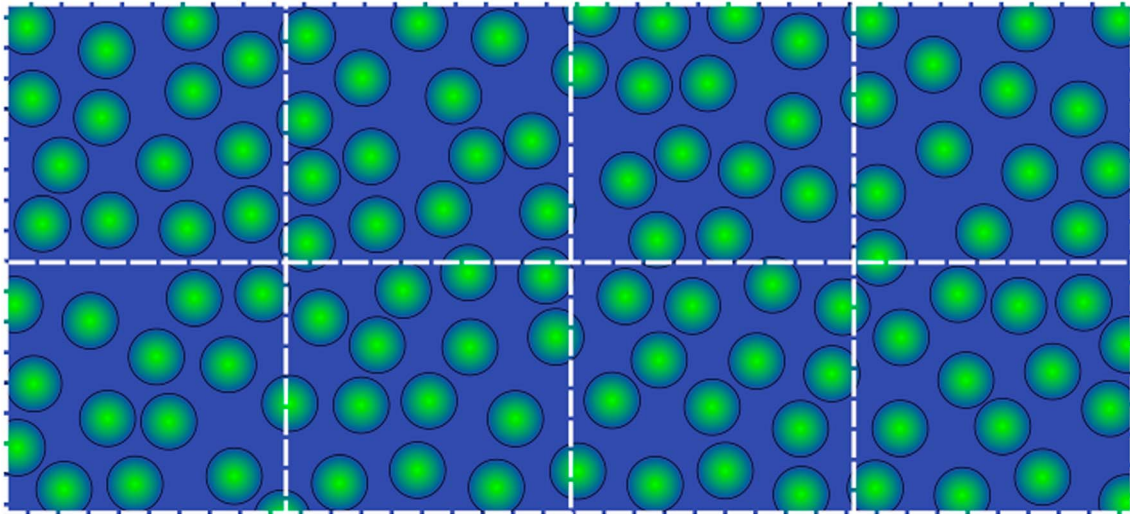


Figure 1. Consistent with the conceptual foundation of the radiative transfer theory, a regolith surface is modeled as consisting of elementary volumes randomly populated by particles.

Although it could be more mathematically rigorous to use the cubical (rather than spherical) shape of an elementary volume (cf. Figure 1), the quantitative effect of doing that becomes negligible upon statistical averaging over all particle positions within the volume (Tishkovets & Petrova, 2013a, 2016, 2017). The superposition T-matrix method solves the macroscopic Maxwell equations for the cluster as a whole. Therefore, near-field effects within the cluster, which are important to capture when modeling densely packed particulate media, are automatically incorporated. The computation is done with the Multiple Sphere T-Matrix (MSTM) program (Mackowski & Mishchenko, 1996, 2011) run on the Pleiades Supercomputer at National Aeronautics and Space Administration (NASA) Ames Center and the SeaWulf and Lired clusters at Stony Brook University. Although the Maxwell equations are always solved for a fixed cluster, the MSTM program subsequently averages the cluster scattering characteristics over all cluster orientations, thereby effectively accomplishing the requisite task of averaging over all particle positions within the elementary volume (Mishchenko, 2014; Mishchenko, Dlugach, et al., 2016).

The MSTM program requires particle positions within the initial cluster, complex indices of refraction, and size parameters as inputs. The particle size parameter is defined as $2\pi r/\lambda$, where r is the particle radius and λ is the wavelength in the surrounding medium. A collision-driven molecular dynamics algorithm (Donev et al., 2005) was used to generate the positions of 1,000 individual particles each having a diameter of $3.3 \mu\text{m}$. The complex indices of refraction of a common igneous mineral, enstatite, across midinfrared wavelengths from Rucks and Glotch (2014) were used, with contribution percentages of each of the three principal indices of refraction following Ito et al. (2017). The choice of the mineral and of the individual particle diameter used here represents some of the frequently encountered compositions and smallest particle size fractions for planetary regoliths (Carrier et al., 1991; Gundlach & Blum, 2013; McKay et al., 1991; Papike et al., 1991). As to the choice of the number of particles in a cluster, increasing this number during the MSTM computation generally leads to modeled spectra increasingly consistent with laboratory measured spectra (Ito et al., 2017); however, the improvements are minor after about 1,000 particles. Furthermore, the number of particles was chosen to be 1,000 to maintain enough dense packing near-field effects captured by the superposition T-matrix method. Additionally, 1,000-particle clusters preserve the balance between improvements in modeled spectra and the increasing computational burden with the use of more particles. We investigate midinfrared wavelengths in this work as the analytical methods for this wavelength range require substantial improvement when analyzing spectra of fine-grained regolith surfaces (e.g., Ramsey & Christensen, 1998; Rogers et al., 2007; Thorpe et al., 2015).

2.2. Static Structure Factor Correction

Ito et al. (2017) observed that the use of the superposition T-matrix method to compute the single-scattering characteristics of an elementary volume results in a spurious forward-scattering feature, wherein the magnification of the “diffraction” peak caused by the far-field effect of forward-scattering interference (Mishchenko,

2014) becomes exceedingly strong. This feature is inconsistent with existing evidence that packing-density effects serve to suppress rather than enhance the diffraction peak of individual particles and hence weaken the forward-scattering phase function of an elementary particulate volume (see Mishchenko, 1994, and references therein). The explanation of this paradox is that the T-matrix technique incorporates the far-field forward-scattering interference effect by definition, whereas this effect does not manifest itself in near-field scattering interactions between adjacent elementary volumes. In order to counteract this problem and better model the scattering pattern relevant to an elementary volume of particulate medium, we apply the static structure factor correction (Mishchenko, 1994; Mishchenko & Macke, 1997; Tsang et al., 1985) to the cluster scattering parameters obtained from the T-matrix method.

The static structure factor correction arises from the treatment of the mutual influence of particles on each other's positions in terms of what is known as the pair-distribution function. According to this approach, the position of one particle is influenced directly by the presence of an immediate neighboring particle and indirectly by the presence of the sum of all the other particles. This signifies that the filling factors (packing density) of the particles, along with their size (radius for spherical particles), are key factors in determining how closely spaced together the particles are on average and therefore govern the pair-distribution function. The pair-distribution function can be translated to the static structure factor by a method known as the Percus-Yevick approximation, which assumes that the particles are impenetrable, spherical, and nearly equal-sized. With the incorporation of the static structure factor, one accounts for the effect of nonrandom particle positions on the interference of the waves singly scattered by the individual particles within an elementary volume, the main result being the suppression of forward scattering by the entire volume.

The static structure factor correction has been applied to spectral studies of silica and snow particulate media (Chen et al., 2014; Cheng et al., 2010; Huang et al., 2016; Pitman et al., 2005; Reichardt & Kulp, 2016), though these applications used single-particle Mie and spheroid T-matrix methods (Mishchenko et al., 1996, 1997, 2002). Our approach combines the superposition T-matrix method and the static structure factor correction, essentially accounting for the fact that the far-field diffraction peak of an isolated elementary volume rendered by the T-matrix procedure cannot manifest itself in a particulate medium.

In this study, the packing density of particles inside an elementary volume (and thus throughout the regolith layer) used during the T-matrix and the static structure factor computations are kept at 0.2, which falls within the range of reported packing densities of lunar regolith (0.13–0.26; Hapke & Sato, 2016; Ohtake et al., 2010). Additionally, the packing density of 0.4 is tested to observe the effects of denser packing. The technical details of the static structure factor correction, its scope, and a FORTRAN program for its practical implementation are described in the Appendix A.

2.3. Radiative Transfer Model

The final, third component of our modeling approach is the use of the above-discussed single-scattering characteristics of elementary volumes to compute the reflectivity and emissivity of the entire particulate layer with the RTT. For the purposes of this study, we assume that the scalar approximation of radiative transfer is sufficiently accurate in the resonance region of particle sizes relative to the wavelength (Mishchenko et al., 2006). Accordingly, we utilize the invariant-embedding solution to the scalar radiative transfer equation for a macroscopically flat, homogeneous, and optically semi-infinite particulate medium (Mishchenko et al., 1999) as a reasonable substitute for the more laborious rigorous treatment with full account of polarization (Mishchenko et al., 2015). Here the Fourier-decomposed Ambartsumian nonlinear integral equation

$$\begin{aligned}
 (\mu + \mu_0)R^m(\mu, \mu_0) &= \frac{\varpi}{4}P^m(-\mu, \mu_0) \\
 &+ \frac{\varpi}{2}\mu_0 \int_0^1 P^m(\mu, \mu')R^m(\mu', \mu_0) d\mu' \\
 &+ \frac{\varpi}{2}\mu \int_0^1 R^m(\mu, \mu')P^m(\mu', \mu_0) d\mu' \\
 &+ \varpi\mu\mu_0 \int_0^1 \int_0^1 R^m(\mu, \mu')P^m(-\mu', \mu'')R^m(\mu'', \mu_0) d\mu' d\mu''
 \end{aligned} \tag{1}$$

is solved numerically using the method of iterations, where μ_0 is the cosine of the incident angle, μ is the cosine of the reflection angle, ϖ is the single-scattering albedo, R^m is the m th Fourier component of the

bidirectional reflection function, and P^m is the m th Fourier component of the phase function. Both ϖ and P^m represent the single-scattering characteristics of an elementary volume. Integrated reflection values, plane (A_P) and spherical (A_S) albedos, are obtained as

$$A_P(\mu_0) = 2 \int_0^1 R^0(\mu, \mu_0) \mu \, d\mu \quad (2)$$

and

$$A_S = 2 \int_0^1 A_P(\mu_0) \mu_0 \, d\mu_0, \quad (3)$$

respectively. Here A_S is equivalent to the hemispherically integrated reflectance, R . The advantage of the computation of reflectivity with this approach is that the solution to the scalar radiative transfer equation is numerically exact while being fast, thereby maintaining practical simplicity and posing no serious computational obstacles to modern desktop computers. Additionally, commonly used parameters in subjects of light scattering, the single-scattering albedo and generalized spherical function expansion coefficients of the scattering matrix elements (refer to Appendix A) are utilized, which allow this method to be used in concert with inputs from a variety of sources.

In the midinfrared wavelengths, spectra of hemispherically integrated emissivities are commonly used. The hemispherical emissivity, ε , is the complement of the spherical albedo (A_S or R) for a semi-infinite particulate medium according to Kirchhoff's law as $\varepsilon = 1 - A_S$ (Hapke, 1993; Salisbury, 1993). Furthermore, integrated values, such as the spherical albedo and hemispherical emissivity, are the most suitable values to be modeled using our approach as other quantities, like bidirectional reflectance and polarization, are difficult to model correctly due to the assumption of spherical particles implemented in the superposition T-matrix and static structure factor procedures (Mishchenko, 2014). We compute the hemispherical emissivity at 10 cm^{-1} intervals within the 400 to $1,500 \text{ cm}^{-1}$ (6.67 to $25.0 \text{ }\mu\text{m}$) range with appropriate single-scattering albedo and generalized spherical function expansion coefficients from the superposition T-matrix and static structure factor correction methods as elementary-volume inputs.

3. Results

Modeled emissivity spectra of an enstatite particulate medium with 0.2 and 0.4 packing densities are shown in Figure 2. The implementation of the static structure factor correction increased emissivity at all wavelengths except for the Christiansen feature at $\sim 1,200 \text{ cm}^{-1}$ where no change is observed.

At a packing density of 0.2, the implementation of the static structure factor correction results in a better fit to the laboratory spectrum of an enstatite powder reported by Ito et al. (2017) than the spectrum modeled solely with the superposition T-matrix method (Figure 2). The quality of agreement is wavelength dependent, and therefore, agreements should be analyzed in sections of the whole wavelength range covered here. The agreement of the modeled emissivities with the laboratory counterpart at some of the most important spectral feature wavelength ranges is summarized as root-mean-square errors in Table 1. The $700\text{--}900 \text{ cm}^{-1}$ region, known as the transparency feature, is a predominant spectral feature for this particle size fraction, but has faced considerable modeling difficulties in the past. Here the transparency feature is particularly well modeled by the implementation of the static structure factor correction at the packing density 0.2.

At a packing density of 0.4, the use of the static structure factor correction produced a spectrum with low spectral contrast compared to the laboratory spectrum (Figure 2). The agreement is worse compared to the case of the 0.2 packing density, and furthermore, the agreement is worse than the spectrum computed solely with the superposition T-matrix method (Table 1). At frequencies higher than the Christiansen feature ($1,200 \text{ cm}^{-1}$), the use of the static structure factor correction at the 0.4 packing density led to the best agreeing modeled spectrum among the ones computed in this study, though the fit is still poor. The overall poor fit also is observed at the shortest frequencies ($< 450 \text{ cm}^{-1}$).

4. Discussion

The static structure factor correction is best suited for relatively low packing densities and when coupled with the superposition T-matrix method. For a low packing density (0.2), the spectrum is modeled well at many

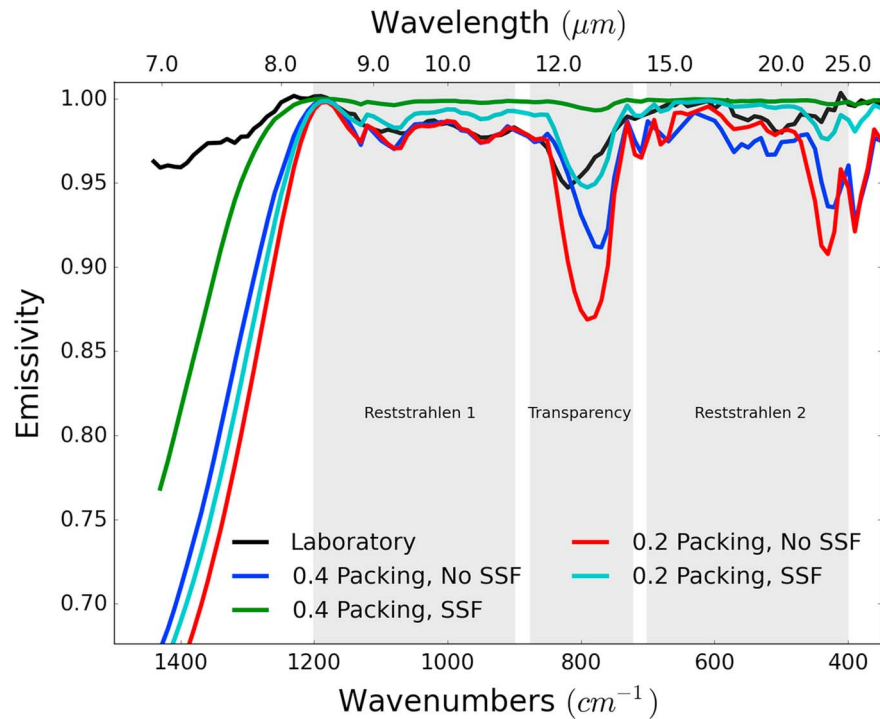


Figure 2. Modeled emissivity spectra of enstatite particulate medium. Packing density in the T-matrix cluster procedure and static structure factor (SSF) correction is varied. The spectral resolution of the laboratory measurement has been adjusted to that of the modeled spectra (10 cm^{-1} intervals). Highlighted regions labeled Reststrahlen 1, Reststrahlen 2, and Transparency approximately indicate the wavelength ranges where root-mean-square errors were calculated.

frequencies, particularly at the transparency feature. This is important for studies of many solar system bodies as the regolith particles are thought to be gently deposited on surfaces with packing densities close to 0.2, as for the case of lunar regolith (Hapke & Sato, 2016; Ohtake et al., 2010). The capability to accurately model spectral features is essential as mineralogical analysis based on spectroscopy relies heavily on the magnitudes and shapes of major spectral features.

For higher packing densities, the static structure factor correction leads to an overcorrection of spectral contrast at all wavelengths (except at the Christiansen feature). Such featureless spectra will likely not be useful in mineralogical analysis, and therefore, the static structure factor correction would not provide benefits at high packing densities.

The behavior of emissivity spectra with varying packing densities can be further understood by examining the single-scattering parameters of an elementary volume: the single-scattering albedo (ω) and phase function (a_1).

Table 1

Root-Mean-Square Errors Showing the Agreement Between Modeled and Laboratory Spectra at Three Distinctive Wavelength Regions

Packing density	Static structure factor correction	Wavelength region		
		Reststrahlen 1	Reststrahlen 2	Transparency
0.2	No	0.00495	0.05701	0.03123
	Yes	0.00781	0.01235	0.00844
0.4	No	0.00452	0.02582	0.02471
	Yes	0.01501	0.02912	0.00997

Note. The wavelength (wavenumber) regions are Reststrahlen 1: $900\text{--}1,200\text{ cm}^{-1}$, Reststrahlen 2: $400\text{--}700\text{ cm}^{-1}$, and Transparency: $700\text{--}900\text{ cm}^{-1}$. The lowest root-mean-square values for each of the three categories are indicated with bold characters.

Table 2
Single-Scattering Albedos for the Selected Wavenumbers in the Defined Wavelength Regions

Packing density	Static structure factor correction	Wavelength region		
		Reststrahlen 1	Reststrahlen 2	Transparency
0.2	No	0.4919	0.4799	0.7789
	Yes	0.1771	0.1637	0.4513
0.4	No	0.5062	0.4974	0.6488
	Yes	0.0422	0.0390	0.0767

Note. Reststrahlen 1: 989.30 cm^{-1} , Reststrahlen 2: 530.30 cm^{-1} , and Transparency: 800.30 cm^{-1} .

4.1. Single-Scattering Albedo

Reststrahlen features are reflective features (for particles greater than the wavelength) characterized by a large imaginary part of the complex index of refraction. For small particles, that is, this study ($3.3\text{-}\mu\text{m}$ sized particles scattering midinfrared light), at Reststrahlen wavelengths, particles scatter light less efficiently than at transparency wavelengths, leading to lower single-scattering albedos than that for the transparency wavelengths (Table 2). When the packing density is increased in the T-matrix procedure, the single-scattering albedo increases at Reststrahlen wavelengths. At these wavelengths, the incoming light is mostly scattered by the particles located on the outside, or the surface, of the cluster representing an elementary volume. The inner particles do not get much opportunity to interact with incoming light (the so-called shielding effect; e.g., Hapke, 1993; Tishkovets, 2008; Tishkovets & Petrova, 2013b). Lower packing densities lead to easier penetration of light into the cluster, which increases the chance of absorption of light by the particles and hence, leads to lower single-scattering albedos.

The opposite effect is observed for the transparency feature. At transparency wavelengths, increased “volume scattering” is experienced for small particles in which each particle easily transmits and incrementally scatters light so that, in sum, it becomes easier for light to exit the cluster (Hunt & Vincent, 1968; Salisbury & Wald, 1992; Vincent & Hunt, 1968). This yields higher and lower single-scattering albedos and emissivity values, respectively, compared to Reststrahlen wavelengths. Increasing the packing density in the T-matrix procedure reduces the interstitial pore spaces and leads to fewer opportunities for volume scattering to take place; therefore, the cluster single-scattering albedo is lower at the 0.4 packing density than at 0.2 (Table 2). These are some of the manifestations of the near-field effect and are well captured by the superposition T-matrix method (Figure 3).

Increasing the packing density in the static structure factor correction decreases the cluster single-scattering albedo at all wavelengths compared to the cluster single-scattering albedo computed solely by the superposition T-matrix method (Table 2). When comparing the effect of the static structure factor correction with 0.2 and 0.4 packing densities, the cluster single-scattering albedo is lower for the 0.4 packing density than for the 0.2 packing density. The reflective property of the Reststrahlen features (still weakly manifesting with $3.3\text{-}\mu\text{m}$ particle size fraction) is reduced upon the static structure factor correction. While the root-mean-square error is low for the defined Reststrahlen 2 region at 0.2 packing density, the misfit of the Reststrahlen band itself (550 cm^{-1}) is still noticeable (Figure 2) when the static structure factor correction is applied. Similarly, at the transparency feature, the larger packing density in the static structure factor correction leads to lower cluster single-scattering albedos (Table 2). Increasing the packing density with the static structure factor correction reduces the overly reflective property of the clusters due to strong volume scattering at transparency wavelengths.

4.2. Phase Function

The phase function (a_1) characterizes the intensity of the scattered light as a function of scattering angle and is generally strongly peaked in the forward direction (small scattering angles) when using the cluster-based light scattering model of an elementary volume.

Both increasing the packing density with the static structure factor and increasing the particle packing density in the T-matrix procedure decrease the forward-scattering phase function values (Figure 4; see also Figure A1). Increase of packing density has various effects on the backscattering direction (larger scattering angles). When the packing density is increased in the static structure factor correction, larger phase function values are produced in the backscattering direction than those solely modeled by the superposition T-matrix

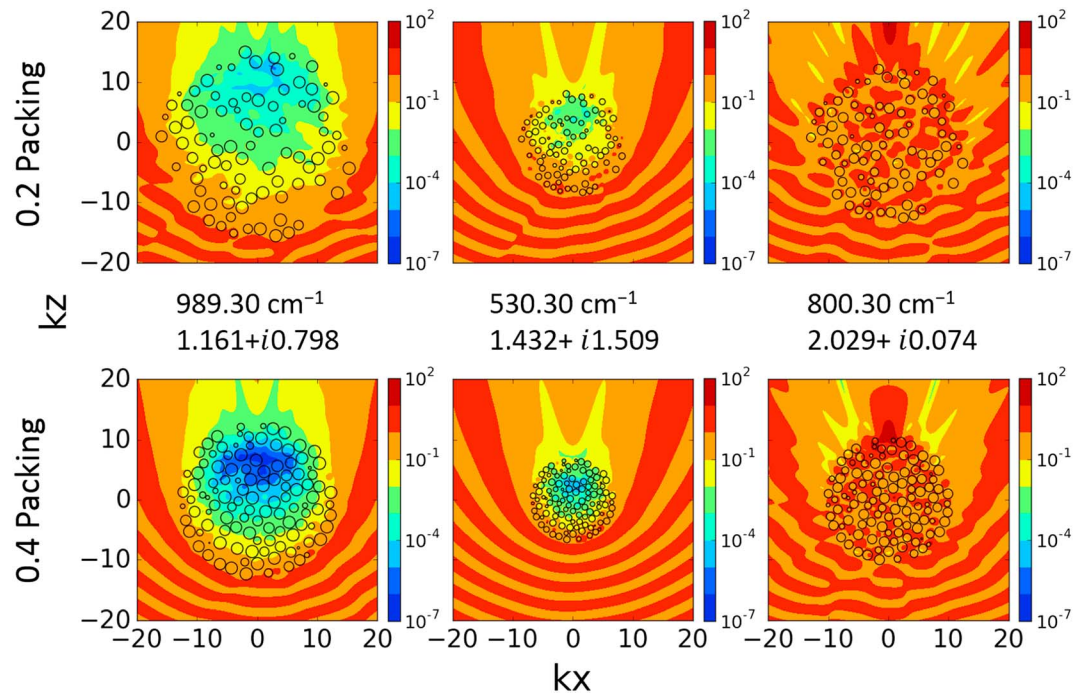


Figure 3. Visualization of light scattering by clusters during the T-matrix procedure. The magnitude of the electric field, $|E^2|$, which is a superposition of the incident and scattered fields (nondimensionalized and unitless), is depicted in color contours. kx and kz are coordinate units relative to the size of the particles and wavelength, that is, the dimensionless size-parameter units. Cross-sectional views through the middle of the clusters are shown, where incident light is propagating from the negative to positive kz direction. Top and bottom rows show packing densities of 0.2 and 0.4, respectively. Selected frequencies are 989.30 cm^{-1} (Reststrahlen 1 region), 530.30 cm^{-1} (Reststrahlen 2 region), and 800.30 cm^{-1} (Transparency region); they are arranged in columns from left to right. The complex indices of refraction for each frequency are shown. The electric field magnitude inside the clusters is higher at 800.30 cm^{-1} than at either 989.30 or 530.30 cm^{-1} and propagates more easily through the clusters. These plots capture the characteristics of high volume scattering and surface reflection at transparency and Reststrahlen features, respectively.

method (Figure 4). Increasing the particle packing density in the T-matrix procedure does not seem to have a clear pattern in the outcomes of phase function values in the backscattering direction.

4.3. Model Discrepancies

Major modeling difficulty arises at short wavelengths. A sharp drop in emissivity is observed for all modeled spectra at $>1,300 \text{ cm}^{-1}$ ($<7.69 \mu\text{m}$). Increasing the cluster packing density in the static structure factor corrects this problem to some degree and emissivity increases (Figure 2). The correction at these wavelengths is not remarkable as even though the intensity is increased, the improper spectral shape is maintained, and the modeled spectra do not come substantially closer in agreement with the laboratory spectrum. As discussed in Ito et al. (2017), diffraction effects at high frequencies may not be subdued enough with a computationally limited number of particles (1,000) used in clusters to accurately model the laboratory spectrum. This discrepancy may also be attributed to the use of monodisperse particles (equal-sized spheres) in the clusters as opposed to actual polydisperse and potentially nonspherical particles, though modeling with such particles is more complex and out of scope for this work. We note that the difficulty in accurately modeling spectra of densely packed media at short wavelengths (particle size parameter near 1) has also been a problem for other RT-based approaches (e.g., Ramezanpour & Mackowski, 2017). Additionally, large variations in fit accuracies are observed for most models at shortest frequencies ($<450 \text{ cm}^{-1}$), likely due to the difficulty in obtaining accurate complex indices of refraction.

5. Conclusions

This work investigated a radiative transfer model for densely packed particulate media using a combination of the superposition T-matrix method and static structure factor correction to accommodate dense packing effects on the solution of the radiative transfer equation. The superposition T-matrix method captures the

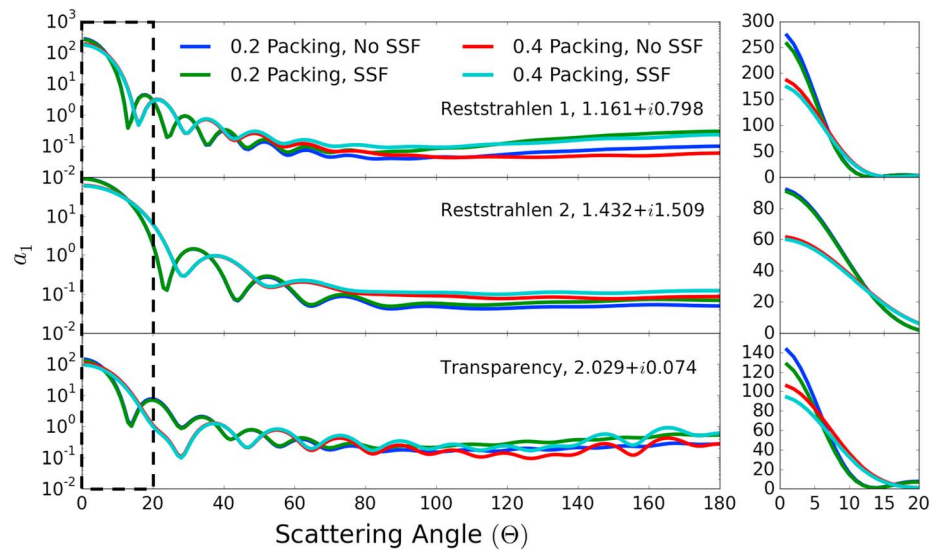


Figure 4. Ensemble-averaged phase function of the cluster, a_1 , at various packing densities: 989.30 cm^{-1} in the top panel, 530.30 cm^{-1} in the middle panel, and 800.30 cm^{-1} in the bottom panel; they represent the defined Reststrahlen 1, Reststrahlen 2, and Transparency regions, respectively. The complex indices of refraction for each frequency are provided. The right-hand inserts are focused on the first 20° of the scattering angle to emphasize the decrease in the forward scattering peak caused by increase in packing density. SSF indicates static structure factor correction.

near-field effects within the elementary volume of particulate medium, while the static structure factor correction suppresses the undesirable far-field effect of forward-scattering interference. We then demonstrated the importance of proper treatment of the packing-density effects when modeling spectra of semi-infinite densely packed particulate media using the cluster-based light scattering model.

Spectra of an enstatite particulate medium with individual particles having a median diameter of $3.3 \text{ }\mu\text{m}$ at midinfrared wavelengths were modeled. This corresponds to some of the typical situations in remote sensing of regolith-covered planetary surfaces in which proper analyses of spectra have been difficult. Our work contributes to resolving this problem by better understanding packing density effects on spectra.

To test the new light-scattering model, we compared its outcome with the benchmark laboratory spectrum of a corresponding enstatite powder. At a packing density of 0.2, the implementation of the static structure factor correction produced modeled spectra having overall better agreement (dependent on wavelength) with the experimental data than those based on the sole use of the superposition T-matrix method. This demonstrates the virtue of coupling the superposition T-matrix method and the static structure factor correction for analyses of spectra of weakly and moderately packed planetary regoliths. A packing density of 0.4 led to an overly reduced spectral contrast, indicating that the static structure factor correction with high packing densities likely will not provide benefits to interpretations of spectra for the retrieval of material properties.

Specific wavelengths were chosen from some of the most important wavelength regions for spectral studies to examine the single-scattering properties of an elementary volume of particulate medium. Our analysis sheds light on the mechanisms of observed spectral traits. The implementation of the static structure factor correction led to reduction in the single-scattering albedo, reduction in the forward scattering phase-function peak, and increase in backscattering phase-function values obtained from the superposition T-matrix method. This is advantageous at wavelengths where volume scattering is dominant, such as the transparency feature of enstatite (e.g., $\sim 800 \text{ cm}^{-1}$), as the overly reflective nature of the cluster from the T-matrix method was suppressed, and emissivity values that more closely resemble laboratory emissivity values were computed. For Reststrahlen wavelengths (e.g., ~ 530 and $\sim 989 \text{ cm}^{-1}$), our coupling approach may not provide substantial benefits as scattering is excessively reduced. For this reason, the superposition T-matrix and static structure factor coupling method likely will not improve spectral modeling of larger particle sizes (compared to wavelength) as their scattering properties are generally dominated by surface reflections (Reststrahlen features) rather than volume scattering (transparency features). Last, in reducing the unwanted forward scattering phase-function peak, we suspect that using a smaller number of particles in a cluster during the T-matrix

computation may lead to more potent reductions (Figures 4 and A1); in such a case, clusters should still contain enough particles to capture the near-field effects, and more insight into this is a subject of future research.

Appendix A

A1. Radiative Transfer Theory Applied to Densely Packed Media

An efficient method in solving the vector (as well as scalar) radiative transfer equation for a sparse, plane-parallel, macroscopically isotropic, and mirror-symmetric particulate medium composed of randomly oriented particles (Mishchenko & Yurkin, 2017) is to expand the normalized scattering matrix elements of an elementary volume in generalized spherical functions (GSFs; Mishchenko et al., 2002). Furthermore, the expansion of the scattering matrix in GSFs can be corrected for the interference effects caused by nonrandom particle positions in a densely packed elementary volume by using the static structure factor concept. Applications of the RTT to densely packed media are frequently encountered in various disciplines, ranging from Earth and planetary sciences to biology (Mishchenko, Dlugach, et al., 2016). Therefore, access to an efficient and fast computer program that modifies previously obtained GSF expansion coefficients to those corrected for dense-packing interference effects to ultimately solve the radiative transfer equation is often essential. Here we explain the theoretical basis of the correction of an existing GSF expansion with the static structure factor, describe the corresponding public-domain FORTRAN program, and show examples of using this program.

A2. Scattering Matrix and Generalized Spherical Function Expansions

The particulate scattering medium is assumed to be ergodic and macroscopically isotropic and mirror-symmetric, thereby leading to the full characterization of its single-scattering properties with the ensemble-averaged single scattering albedo, ω , and normalized 4×4 Stokes scattering matrix, $\tilde{\mathbf{F}}(\theta)$, of an elementary volume (Mishchenko, 2014). The normalized scattering matrix is written as

$$\tilde{\mathbf{F}}(\theta) = \begin{bmatrix} a_1(\theta) & b_1(\theta) & 0 & 0 \\ b_1(\theta) & a_2(\theta) & 0 & 0 \\ 0 & 0 & a_3(\theta) & b_2(\theta) \\ 0 & 0 & -b_2(\theta) & a_4(\theta) \end{bmatrix} \quad (\text{A1})$$

with the scattering angle spanning the range $\theta \in [0, \pi]$. The (1,1) element of the scattering matrix, known as the phase function, satisfies the normalization condition

$$\frac{1}{2} \int_0^\pi d\theta \sin\theta a_1(\theta) = 1. \quad (\text{A2})$$

The scattering matrix elements are expanded using GSFs, $P_{mn}^s(\cos\theta)$, as

$$a_1(\theta) = \sum_{s=0}^{s_{\max}} \alpha_1^s P_{00}^s(\cos\theta), \quad (\text{A3})$$

$$a_2(\theta) + a_3(\theta) = \sum_{s=0}^{s_{\max}} (\alpha_2^s + \alpha_3^s) P_{22}^s(\cos\theta), \quad (\text{A4})$$

$$a_2(\theta) - a_3(\theta) = \sum_{s=0}^{s_{\max}} (\alpha_2^s - \alpha_3^s) P_{2,-2}^s(\cos\theta), \quad (\text{A5})$$

$$a_4(\theta) = \sum_{s=0}^{s_{\max}} \alpha_4^s P_{00}^s(\cos\theta), \quad (\text{A6})$$

$$b_1(\theta) = \sum_{s=0}^{s_{\max}} \beta_1^s P_{02}^s(\cos\theta), \quad (\text{A7})$$

$$b_2(\theta) = \sum_{s=0}^{s_{\max}} \beta_2^s P_{02}^s(\cos\theta), \quad (\text{A8})$$

where s_{\max} is the upper summation limit defined by the requisite numerical accuracy of the series. Alternatively, the expansions (A3)–(A8) can be reformulated in terms of Wigner d -functions (Mishchenko, 2014),

$$d_{mn}^s(\theta) = i^{n-m} P_{mn}^s(\cos\theta). \quad (\text{A9})$$

When the scattering matrix elements are already known and the expansion coefficients are needed, the following formulas following from the orthogonality property of the Wigner d -functions can be used:

$$\alpha_1^s = \left(s + \frac{1}{2}\right) \int_0^\pi d\theta \sin\theta a_1(\theta) d_{00}^s(\theta), \quad (\text{A10})$$

$$\alpha_2^s + \alpha_3^s = \left(s + \frac{1}{2}\right) \int_0^\pi d\theta \sin\theta [a_2(\theta) + a_3(\theta)] d_{22}^s(\theta), \quad (\text{A11})$$

$$\alpha_2^s - \alpha_3^s = \left(s + \frac{1}{2}\right) \int_0^\pi d\theta \sin\theta [a_2(\theta) - a_3(\theta)] d_{2,-2}^s(\theta), \quad (\text{A12})$$

$$\alpha_4^s = \left(s + \frac{1}{2}\right) \int_0^\pi d\theta \sin\theta a_4(\theta) d_{00}^s(\theta), \quad (\text{A13})$$

$$\beta_1^s = -\left(s + \frac{1}{2}\right) \int_0^\pi d\theta \sin\theta b_1(\theta) d_{02}^s(\theta), \quad (\text{A14})$$

$$\beta_2^s = -\left(s + \frac{1}{2}\right) \int_0^\pi d\theta \sin\theta b_2(\theta) d_{02}^s(\theta). \quad (\text{A15})$$

In practice, the integrals in equations (A10)–(A15) are computed numerically using a Gaussian quadrature with the number of Gaussian nodes equal to twice the number of the expansion coefficients, s_{\max} . This can be written as

$$\alpha_1^s \approx \left(s + \frac{1}{2}\right) \sum_{j=1}^{N_G} w_j a_1(\arccos\mu_j) d_{00}^s(\arccos\mu_j), \quad (\text{A16})$$

$$\alpha_2^s + \alpha_3^s \approx \left(s + \frac{1}{2}\right) \sum_{j=1}^{N_G} w_j [a_2(\arccos\mu_j) + a_3(\arccos\mu_j)] d_{22}^s(\arccos\mu_j), \quad (\text{A17})$$

$$\alpha_2^s - \alpha_3^s \approx \left(s + \frac{1}{2}\right) \sum_{j=1}^{N_G} w_j [a_2(\arccos\mu_j) - a_3(\arccos\mu_j)] d_{2,-2}^s(\arccos\mu_j), \quad (\text{A18})$$

$$\alpha_4^s \approx \left(s + \frac{1}{2}\right) \sum_{j=1}^{N_G} w_j a_4(\arccos\mu_j) d_{00}^s(\arccos\mu_j), \quad (\text{A19})$$

$$\beta_1^s \approx -\left(s + \frac{1}{2}\right) \sum_{j=1}^{N_G} w_j b_1(\arccos\mu_j) d_{02}^s(\arccos\mu_j), \quad (\text{A20})$$

$$\beta_2^s \approx -\left(s + \frac{1}{2}\right) \sum_{j=1}^{N_G} w_j b_2(\arccos\mu_j) d_{02}^s(\arccos\mu_j), \quad (\text{A21})$$

where μ_j and w_j are the Gaussian quadrature nodes and weights on the interval $[-1, 1]$ and $N_G = 2s_{\max}$. The Wigner d -functions are computed with the recurrence relation

$$d_{mn}^{s+1}(\theta) = \frac{1}{s\sqrt{(s+1)^2 - m^2}\sqrt{(s+1)^2 - n^2}} \times \left\{ (2s+1)[s(s+1)\cos\theta - mn]d_{mn}^s(\theta) - (s+1)\sqrt{s^2 - m^2}\sqrt{s^2 - n^2}d_{mn}^{s-1}(\theta) \right\}, \quad (\text{A22})$$

where $s \geq s_{\min}$ and

$$s_{\min} = \max(|m|, |n|). \quad (\text{A23})$$

The initial values are given by

$$d_{mn}^{s_{\min}-1}(\theta) = 0, \quad (\text{A24})$$

$$d_{mn}^{s_{\min}}(\theta) = \zeta_{mn} 2^{-s_{\min}} \left[\frac{(2s_{\min})!}{(|m-n|)! (|m+n|)!} \right]^{1/2} \times (1 - \cos\theta)^{|m-n|/2} (1 + \cos\theta)^{|m+n|/2}, \quad (\text{A25})$$

where

$$\zeta_{mn} = \begin{cases} 1 & \text{for } n \geq m, \\ (-1)^{m-n} & \text{for } n < m. \end{cases} \quad (\text{A26})$$

A3. Static Structure Factor Correction

The static structure factor accounts for the statistics of mutual positions of particles in densely packed media. Aside from the filling factor (packing density), the static structure factor is dependent on scattering angle, particle size distribution, particle shape, and wavelength. We assume that the particles are nearly spherical and nearly monodisperse (Mishchenko, 1994). The Percus-Yevick approximation for hard, impenetrable, monodisperse spheres gives the static structure factor, $S(\theta)$, as

$$S(\theta) = \frac{1}{1 - nC(p)} \quad (\text{A27})$$

and

$$p = [4\pi(\theta/2)]/\lambda \quad (\text{A28})$$

where n is the number density of scattering particles and λ is wavelength. When p equals zero,

$$C(0) = -24 \frac{f}{n} \left(\frac{\alpha}{3} + \frac{\beta}{4} + \frac{\delta}{6} \right), \quad (\text{A29})$$

while for nonzero values

$$C(p) = 24 \frac{f}{n} \left[\frac{\alpha + \beta + \delta}{u^2} \cos u - \frac{\alpha + 2\beta + 4\delta}{u^3} \sin u - \frac{2(\beta + 6\delta)}{u^4} \cos u + \frac{2\beta}{u^4} + \frac{24\delta}{u^5} \sin u + \frac{24\delta}{u^6} (\cos u - 1) \right], \quad p \neq 0. \quad (\text{A30})$$

In the above equations for C ,

$$u = 2pr_0 \quad (\text{A31})$$

$$\alpha = \frac{(1 + 2f)^2}{(1 - f)^4} \quad (\text{A32})$$

$$\beta = -6f \frac{(1 + f/2)^2}{(1 - f)^4} \quad (\text{A33})$$

$$\delta = \alpha f / 2 \quad (\text{A34})$$

where r_0 is the radius of a particle and f is the filling factor expressed as

$$f = \frac{4}{3} \pi n r_0^3 \quad (\text{A35})$$

To apply the static structure factor correction, the scattering cross section, C_{sca} , accompanying the input expansion coefficients of the normalized scattering matrix is first modified as

$$C_{\text{sca,ssf}} = \int_{4\pi} d\Omega \frac{dC_{\text{sca}}}{d\Omega} S(\theta) \quad (\text{A36})$$

where the differential scattering cross section

$$\frac{dC_{\text{sca}}}{d\Omega} = \frac{C_{\text{sca}}}{4\pi} a_1(\theta) \quad (\text{A37})$$

(subscript *ssf* stands for static structure factor corrected). The integral is evaluated again using the Gaussian quadrature with the number of nodes (scattering angles) equal to twice the number of input expansion coefficients. The original expansion coefficients are used to compute the normalized scattering matrix elements

Table A1
Sample Input File

2.84241	0.26479	2.57762	22		
1.00000	0.00000	0.00000	0.81320	0.00000	0.00000
1.83207	0.00000	0.00000	1.85865	0.00000	0.00000
2.35169	3.60749	3.24812	2.19642	-0.24690	0.12802
2.04559	2.56991	2.55723	2.20539	-0.03994	-0.00727
2.35381	2.71119	2.33858	2.16228	-0.20968	0.12005
2.31545	2.37021	2.41555	2.48478	-0.04175	-0.04276
2.61512	2.90036	2.60402	2.46585	-0.13348	0.08688
2.82563	2.72898	2.82540	3.08825	-0.05563	-0.08517
3.10962	3.47152	3.10179	2.91323	-0.25304	-0.13065
3.20155	3.08711	3.28649	3.59939	-0.26278	-0.13667
2.82940	3.43175	3.20887	2.92971	-0.72487	-0.97094
2.00599	2.16514	2.04553	2.21437	-0.16432	-1.13279
1.16690	1.63687	1.03695	0.75345	0.24445	-1.16624
0.04586	0.03523	0.00139	0.03028	0.24515	-0.01131
0.06431	0.07846	0.05853	0.05090	0.03167	-0.01561
0.01468	0.01793	0.01418	0.01206	0.00797	-0.00347
0.00258	0.00315	0.00250	0.00212	0.00161	-0.00049
0.00038	0.00046	0.00035	0.00030	0.00027	-0.00005
0.00005	0.00006	0.00004	0.00004	0.00004	0.00000
0.00001	0.00001	0.00000	0.00000	0.00000	0.00000
0.00000	0.00000	0.00000	0.00000	0.00000	0.00000
0.00000	0.00000	0.00000	0.00000	0.00000	0.00000

Note. From left to right, the first row contains the extinction, absorption, and scattering cross sections plus the number of low-density GSF expansion coefficients. From the second row on, expansion coefficients from $s = 0$ to 21 are shown. The coefficients are α_1 , α_2 , α_3 , α_4 , β_1 , and β_2 from left to right columns. The cross sections and expansion coefficients were generated with the monodisperse Mie method from Mishchenko et al. (2002) using 1.2 μm diameter, 0.63 μm wavelength, and real and imaginary parts of refractive index of 1.530 and 0.008, respectively, corresponding to very weakly absorbing glass in the visible light.

according to equations (A3)–(A8), then the normalization is reversed. The static structure factor is multiplied to the nonnormalized scattering matrix elements as

$$\tilde{\mathbf{F}}_{ssf}(\theta) = \frac{4\pi}{C_{sca,ssf}} \mathbf{F}(\theta) S(\theta) \quad (\text{A38})$$

Using the static structure factor corrected normalized scattering matrix elements, the resulting GSF expansion coefficients are finally computed with equations (A10)–(A15). Finally, we note that the static structure factor correction does not modify the absorption cross section.

A4. Computer Program

The static structure factor correction has been implemented in a FORTRAN program, which can be obtained from the first author upon request or downloaded from <https://www.giss.nasa.gov/staff/mmishchenko/brf/PackedMedia.f>. Input to this program (Table A1) is a file containing the extinction, absorption, and scattering cross sections; the coefficients of the GSF expansions; and the number of the expansion coefficients. These quantities can be obtained, for example, using exact solvers of Maxwell equations, such as the Mie (Mishchenko et al., 2002), T-matrix (Mishchenko et al., 2002), and superposition T-matrix (Mackowski & Mishchenko, 2011) methods. Alternatively, when the scattering matrix is available but not the corresponding GSF expansion coefficients, as in a laboratory measurement (e.g., the average scattering matrix of volcanic ash particles suspended in air; Muñoz et al., 2004), the numerical procedure from Mishchenko, Geogdzhayev, and Yang (2016) can be used to obtain the corresponding GSF expansion coefficients.

The output contains the new single-scattering albedo, the number of new expansion coefficients, and the new expansion coefficients that have been corrected by the static structure factor procedure (Table A2). The output is ready to be further used in radiative transfer models, for example, those described in Mishchenko et al. (1999, 2015).

Table A2
Output File Generated From the Input File in Table A1

0.87720	43				
1.00000	0.00000	0.00000	0.74467	0.00000	0.00000
1.43441	0.00000	0.00000	1.46864	0.00000	0.00000
1.50572	3.14149	2.65268	1.29731	-0.33733	0.20024
0.54855	1.17599	1.15803	0.77997	-0.05930	0.04624
0.53618	0.93526	0.42101	0.29439	-0.28560	0.24569
0.15686	0.14711	0.20261	0.41609	-0.04820	0.06012
0.36933	0.66451	0.24499	0.18811	-0.15777	0.27199
0.57785	0.35170	0.47412	0.96315	-0.03832	0.07655
1.04138	1.42494	0.91249	0.80178	-0.29723	0.04728
1.43661	1.15526	1.41074	1.99388	-0.28707	0.06245
1.38072	2.06382	1.72864	1.49775	-0.88440	-1.06159
0.77632	0.86281	0.67159	1.01182	-0.09748	-1.27747
0.10445	0.62844	-0.19868	-0.52154	0.46542	-1.31238
-1.04618	-1.16241	-1.18892	-1.12413	0.45648	0.26939
-0.73759	-0.80468	-0.79180	-0.80341	0.14217	0.26695
-0.58212	-0.65566	-0.60294	-0.61615	0.08731	0.28520
-0.40919	-0.47367	-0.40752	-0.42301	0.05108	0.27611
-0.24227	-0.29727	-0.22556	-0.23630	0.02282	0.25314
-0.07639	-0.11896	-0.05332	-0.05894	0.00069	0.21416
0.06957	0.04058	0.10195	0.10141	-0.02940	0.16619
0.18259	0.16879	0.22548	0.22978	-0.06459	0.09039
0.24329	0.24662	0.28311	0.28840	-0.07887	-0.01142
0.23201	0.24797	0.25458	0.25808	-0.06208	-0.09369
0.16284	0.18262	0.16590	0.16770	-0.03046	-0.12472
0.07404	0.09083	0.06387	0.06481	-0.00263	-0.11181
-0.00274	0.00828	-0.01870	-0.01826	0.01440	-0.07778
-0.05380	-0.04855	-0.07012	-0.07013	0.02179	-0.04017
-0.07800	-0.07733	-0.09157	-0.09197	0.02275	-0.00786
-0.07987	-0.08227	-0.08927	-0.08990	0.01984	0.01592
-0.06583	-0.06986	-0.07060	-0.07126	0.01450	0.03053
-0.04263	-0.04704	-0.04292	-0.04343	0.00772	0.03607
-0.01686	-0.02066	-0.01356	-0.01384	0.00083	0.03328
0.00555	0.00300	0.01090	0.01083	-0.00458	0.02428
0.02045	0.01934	0.02612	0.02617	-0.00746	0.01251
0.02637	0.02649	0.03094	0.03106	-0.00772	0.00140
0.02447	0.02537	0.02719	0.02731	-0.00608	-0.00680
0.01754	0.01875	0.01829	0.01840	-0.00355	-0.01131
0.00883	0.00995	0.00796	0.00804	-0.00101	-0.01255
0.00112	0.00189	-0.00078	-0.00073	0.00092	-0.01142
-0.00379	-0.00346	-0.00602	-0.00601	0.00193	-0.00891
-0.00521	-0.00529	-0.00714	-0.00715	0.00198	-0.00576
-0.00353	-0.00389	-0.00464	-0.00465	0.00123	-0.00243
0.00000	-0.00044	0.00000	0.00000	0.00003	0.00087

Note. The static structure factor correction is applied using a filling factor of 0.2. The first row contains the high-density single-scattering albedo and the number of expansion coefficients. From the second row, the high-density expansion coefficients from $s = 0$ to 42 are shown, where the coefficients are $a_1, a_2, a_3, a_4, \beta_1,$ and β_2 from left to right columns.

A5. Sample Results

Scattering from densely packed particulate media behaves differently compared to sparsely packed media with widely separated particles, in which one manifestation is the suppression of the forward scattering peak and an enhancement in backscattering (Mishchenko, 1994, 2014; Mishchenko & Macke, 1997). This behavior is captured by our static structure factor correction, as shown by the case of monodisperse spherical particles of very weakly absorbing glass in visible light (Figure A1). The phase function, a_1 , in the forward direction decreases rapidly as the filling factor is increased. This behavior is qualitatively similar to incoherent scattering functions introduced by Muinonen et al. (2016). The backscattering directions increase in intensity by very small amounts. Other elements of the scattering matrix ($a_2, a_3, a_4, b_1,$ and b_2) describe the polarization state of the scattered light.

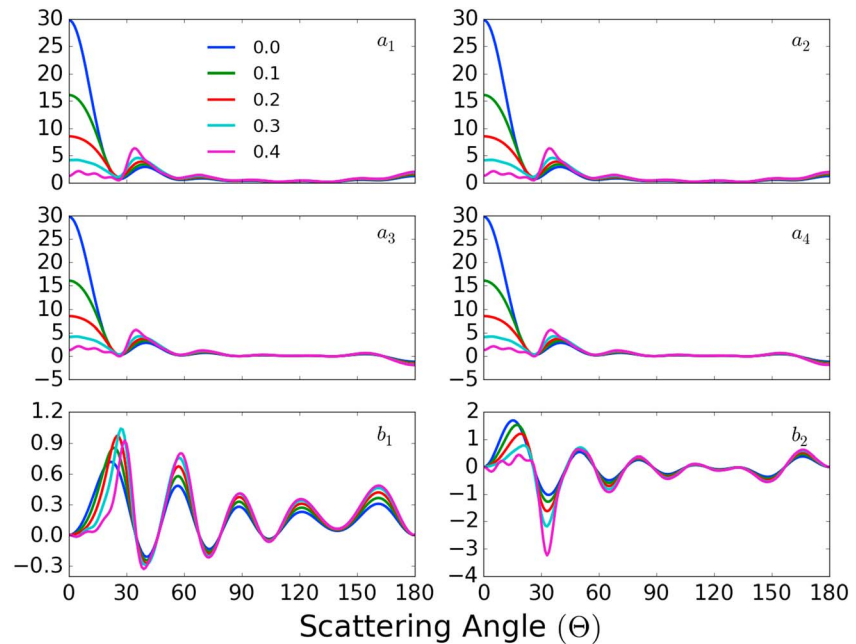


Figure A1. Scattering matrix elements as functions of the scattering angle for filling factors 0.0, 0.1, 0.2, 0.3, and 0.4. The input shown in Table A1 is used.

A6. Future Implementations and Scope

The computer program presented here modifies the scattering cross section and GSF expansion coefficients using the static structure factor correction. The implementation of this program is simple, and we envision that the program will be useful for analyses of planetary regoliths, ice, and other particulate objects encountered in physical, chemical, and biological sciences. However, users must be aware that the static structure factor correction essentially acts as a “patch” to modify the conventional RTT to fit within the working boundaries of densely packed media, and this procedure is not derived from first physical principles, in this case the macroscopic Maxwell equations (Mishchenko, Dlugach, et al., 2016). In general, the a_1 element of the scattering matrix is believed to be the most reliable quantity among the scattering matrix elements. With proper understanding of its scope, we hope that this program will be particularly handy when solving problems related to multiple scattering from densely packed particulate media using radiative transfer and superposition T-matrix methods.

Acknowledgments

G. I. thanks NASA Goddard Institute for Space Studies Internship Program and internship coordinator Matthew D. Pearce. M.I.M. recognizes support from the NASA Radiation Sciences Program and NASA Remote Sensing Theory Program. T. D. G. is supported by the RIS⁴E node of NASA’s Solar System Exploration Research Virtual Institute. This work was funded by New York Space Grant Consortium. We thank Bruce Hapke and an anonymous reviewer for constructive comments on the original manuscript. The data used here are listed in the references and tables. The FORTRAN program used in this work will be uploaded to NASA’s GitHub repository in addition to <https://www.giss.nasa.gov/staff/mmishchenko/brf/PackedMedia.f>.

References

- Carrier, W. D., Olhoef, G. R., & Mendell, W. (1991). Physical properties of the lunar surface. In G. H. Heiken, D. T. Vaniman, & B. M. French (Eds.), *Lunar Source Book* (pp. 475–594). New York: Cambridge University Press.
- Chandrasekhar, S. (1950). *Radiative transfer*. Oxford: Oxford University Press.
- Chen, X., Huang, X., & Flanner, M. G. (2014). Sensitivity of modeled far-IR radiation budgets in polar continents to treatments of snow surface and ice cloud radiative properties. *Geophysical Research Letters*, *41*, 6530–6537. <https://doi.org/10.1002/2014GL061216>
- Cheng, J., Liang, S., Weng, F., Wang, J., & Li, X. (2010). Comparison of radiative transfer models for simulating snow surface thermal infrared emissivity. *IEEE Journal of Selected Topics in Applied Earth Observations and Remote Sensing*, *3*(3), 1939–1940.
- Christensen, P. R., Bandfield, J. L., Hamilton, V. E., Ruff, S. W., Kieffer, H. H., Titus, T. N., et al. (2001). Mars Global Surveyor Thermal Emission Spectrometer experiment: Investigation description and surface science results. *Journal of Geophysical Research*, *106*, 23,823–23,871. <https://doi.org/10.1029/2000JE001370>
- Clancy, R. T., Wolff, M. J., & Christensen, P. R. (2003). Mars aerosol studies with the MGS TES emission phase function observations: Optical depths, particle sizes, and ice cloud types versus latitude and solar longitude. *Journal of Geophysical Research*, *108*, 5098. <https://doi.org/10.1029/2003JE002058>
- Conel, J. E. (1969). Infrared emissivities of silicates: Experimental results and a cloudy atmosphere model of spectral emission from condensed particulate mediums. *Journal of Geophysical Research*, *74*, 1614–1634.
- Dlugach, J. M. (2016). Numerical simulations of electromagnetic scattering by solar system objects. *Journal of Quantitative Spectroscopy and Radiative Transfer*, *183*, 38–55. <https://doi.org/10.1016/j.jqsrt.2016.04.021>
- Dlugach, J. M., & Mishchenko, M. I. (2005). The effect of aerosol shape in retrieving optical properties of cloud particles in the planetary atmospheres from the photopolarimetric data. Jupiter. *Solar System Research*, *39*(2), 102–111. <https://doi.org/10.1007/s11208-005-0026-1>

- Dlugach, J. M., Mishchenko, M. I., Liu, L., & Mackowski, D. W. (2011). Numerically exact computer simulations of light scattering by densely packed, random particulate media. *Journal of Quantitative Spectroscopy and Radiative Transfer*, *112*(13), 2068–2078. <https://doi.org/10.1016/j.jqsrt.2011.02.009>
- Donev, A., Torquato, S., & Stillinger, F. H. (2005). Neighbor list collision-driven molecular dynamics simulation for nonspherical hard particles. I. Algorithmic details. *Journal of Computational Physics*, *202*(2), 737–764. <https://doi.org/10.1016/j.jcp.2004.08.014>
- Feely, K. C., & Christensen, P. R. (1999). Quantitative compositional analysis using thermal emission spectroscopy: Application to igneous and metamorphic rocks. *Journal of Geophysical Research*, *104*, 24,195–24,210. <https://doi.org/10.1029/1999JE001034>
- Glotch, T. D., Bandfield, J. L., Wolff, M. J., Arnold, J. A., & Che, C. (2016). Constraints on the composition and particle size of chloride salt-bearing deposits on Mars. *Journal of Geophysical Research: Planets*, *121*, 454–471. <https://doi.org/10.1002/2015JE004921>
- Gundlach, B., & Blum, J. (2013). A new method to determine the grain size of planetary regolith. *Icarus*, *223*(1), 479–492. <https://doi.org/10.1016/j.icarus.2012.11.039>
- Hapke, B. (1981). Bidirectional reflectance spectroscopy: 1 Theory. *Journal of Geophysical Research*, *86*, 3039–3054. <https://doi.org/10.1029/JB086iB04p03039>
- Hapke, B. (1993). *Theory of reflectance and emittance spectroscopy*. New York: Cambridge University Press. <https://doi.org/10.1017/CBO9780511524998>
- Hapke, B. (2012). *Theory of reflectance and emittance spectroscopy* (2nd ed.). New York: Cambridge University Press.
- Hapke, B., & Sato, H. (2016). The porosity of the upper lunar regolith. *Icarus*, *273*, 75–83. <https://doi.org/10.1016/j.icarus.2015.10.031>
- Huang, X., Chen, X., Zhou, D. K., & Lu, X. (2016). An observationally based global band-by-band surface emissivity dataset for climate and weather simulations. *Journal of the Atmospheric Sciences*, *73*(9), 3541–3555. <https://doi.org/10.1175/JAS-D-15-0355.1>
- Hunt, G. R., & Vincent, R. K. (1968). The behavior of spectral features in the infrared emission from particulate surfaces of various grain sizes. *Journal of Geophysical Research*, *73*, 6039–6046. <https://doi.org/10.1029/JB073i018p06039>
- Ito, G., Arnold, J. A., & Glotch, T. D. (2017). T-matrix and radiative transfer hybrid models for densely packed particulates at mid-infrared wavelengths. *Journal of Geophysical Research: Planets*, *122*, 822–838. <https://doi.org/10.1002/2017JE005271>
- Kolokolova, L., Buratti, B., & Tishkovets, V. (2010). Impact of coherent backscattering on the spectra of icy satellites of Saturn and the implications of its effects for remote sensing. *The Astrophysical Journal*, *711*(2), L71–L74. <https://doi.org/10.1088/2041-8205/711/2/L71>
- Kolokolova, L., Liu, L., Buratti, B., & Mishchenko, M. I. (2011). Modeling variations in near-infrared caused by the coherent backscattering effect. *Journal of Quantitative Spectroscopy and Radiative Transfer*, *112*(13), 2175–2181. <https://doi.org/10.1016/j.jqsrt.2011.03.010>
- Lumme, K., & Bowell, E. (1981a). Radiative transfer in the surfaces of atmosphereless bodies. I. Theory. *The Astronomical Journal*, *86*, 1694–1704. <https://doi.org/10.1086/113054>
- Lumme, K., & Bowell, E. (1981b). Radiative transfer in the surfaces of atmosphereless bodies. II. Interpretation of phase curves. *The Astronomical Journal*, *86*, 1705–1721. <https://doi.org/10.1086/113055>
- Mackowski, D. W. (1994). Calculation of total cross sections of multiple-sphere clusters. *Journal of the Optical Society of America A*, *11*(11), 2851–2861. <https://doi.org/10.1364/JOSAA.11.002851>
- Mackowski, D. W., & Mishchenko, M. I. (1996). Calculation of the T matrix and the scattering matrix for ensembles of spheres. *Journal of the Optical Society of America A*, *13*(11), 2266–2278. <https://doi.org/10.1364/JOSAA.13.002266>
- Mackowski, D. W., & Mishchenko, M. I. (2011). A multiple sphere T-matrix Fortran code for use on parallel computer clusters. *Journal of Quantitative Spectroscopy and Radiative Transfer*, *112*(13), 2182–2192. <https://doi.org/10.1016/j.jqsrt.2011.02.019>
- Maignan, F., Bréon, F.-M., & Lacaze, R. (2004). Bidirectional reflectance of Earth targets: Evaluation of analytical models using a large set of spaceborne measurements with emphasis on the hot spot. *Remote Sensing of Environment*, *90*(2), 210–220. <https://doi.org/10.1016/j.rse.2003.12.006>
- McKay, D. S., Heiken, G., Basu, A., Blanford, G., Simon, S., Reedy, R., et al. (1991). The lunar regolith. In G. H. Heiken, D. T. Vaniman, & B. M. French (Eds.), *Lunar Source Book* (pp. 285–356). New York: Cambridge University Press.
- Mishchenko, M. I. (1990). Physical properties of the upper tropospheric aerosols in the equatorial region of Jupiter. *Icarus*, *84*(2), 296–304. [https://doi.org/10.1016/0019-1035\(90\)90039-C](https://doi.org/10.1016/0019-1035(90)90039-C)
- Mishchenko, M. I. (1994). Asymmetry parameters of the phase function for densely packed scattering grains. *Journal of Quantitative Spectroscopy and Radiative Transfer*, *52*(1), 95–110. [https://doi.org/10.1016/0022-4073\(94\)90142-2](https://doi.org/10.1016/0022-4073(94)90142-2)
- Mishchenko, M. I. (2014). *Electromagnetic scattering by particles and particle groups: An introduction*. Cambridge, UK: Cambridge University Press. <https://doi.org/10.1017/CBO9781139019064>
- Mishchenko, M. I., Dlugach, J. M., Chowdhary, J., & Zakharova, N. T. (2015). Polarized bidirectional reflectance of optically thick sparse particulate layers: An efficient numerically exact radiative-transfer solution. *Journal of Quantitative Spectroscopy and Radiative Transfer*, *156*, 97–108. <https://doi.org/10.1016/j.jqsrt.2015.02.003>
- Mishchenko, M. I., Dlugach, J. M., Yanovitskij, D. G., & Zakharova, N. T. (1999). Bidirectional reflectance of flat, optically thick particulate layers: An efficient radiative transfer solution and applications to snow and soil surfaces. *Journal of Quantitative Spectroscopy and Radiative Transfer*, *63*(2–6), 409–432. [https://doi.org/10.1016/S0022-4073\(99\)00028-X](https://doi.org/10.1016/S0022-4073(99)00028-X)
- Mishchenko, M. I., Dlugach, J. M., Yurkin, M. A., Bi, L., Cairns, B., Liu, L., et al. (2016). First-principles modeling of electromagnetic scattering by discrete and discretely heterogeneous random media. *Physics Reports*, *632*, 1–75. <https://doi.org/10.1016/j.physrep.2016.04.002>
- Mishchenko, M. I., Geogdzhayev, I. V., & Yang, P. (2016). Expansion of tabulated scattering matrices in generalized spherical functions. *Journal of Quantitative Spectroscopy and Radiative Transfer*, *183*, 78–84. <https://doi.org/10.1016/j.jqsrt.2016.05.015>
- Mishchenko, M. I., & Macke, A. (1997). Asymmetry parameters of the phase function for isolated and densely packed spherical particles with multiple internal inclusions in the geometric optics limit. *Journal of Quantitative Spectroscopy and Radiative Transfer*, *57*(6), 767–794. [https://doi.org/10.1016/S0022-4073\(97\)00012-5](https://doi.org/10.1016/S0022-4073(97)00012-5)
- Mishchenko, M. I., Rosenbush, V. K., Kiselev, N. N., Lupishko, D. F., Tishkovets, V. P., Kaydash, V. G., et al. (2010). *Polarimetric remote sensing of solar system objects*. Kyiv, Ukraine: Akadempriodyka. Retrieved from <http://arxiv.org/abs/1010.1171>, <https://doi.org/10.15407/akadempriodyka.134.291>
- Mishchenko, M. I., & Travis, L. D. (1997). Satellite retrieval of aerosol properties over ocean using polarization as well as intensity of reflected sunlight. *Journal of Geophysical Research*, *102*, 16,989–17,013. <https://doi.org/10.1029/96JD02425>
- Mishchenko, M. I., Travis, L. D., Kahn, R. A., & West, R. A. (1997). Modeling phase functions for dustlike tropospheric aerosols using a shape mixture of randomly oriented polydisperse spheroids. *Journal of Geophysical Research*, *102*, 16,831–16,847. <https://doi.org/10.1029/96JD02110>
- Mishchenko, M. I., Travis, L. D., & Laci, A. A. (2002). *Scattering, absorption, and emission of light by small particles*. Cambridge, UK: Cambridge University Press.
- Mishchenko, M. I., Travis, L. D., & Laci, A. A. (2006). *Multiple scattering of light by particles: Radiative transfer and coherent backscattering*. Cambridge, UK: Cambridge University Press.

- Mishchenko, M. I., Travis, L. D., & Mackowski, D. W. (1996). T-matrix computations of light scattering by nonspherical particles: A review. *Journal of Quantitative Spectroscopy and Radiative Transfer*, 55(5), 535–575. [https://doi.org/10.1016/0022-4073\(96\)00002-7](https://doi.org/10.1016/0022-4073(96)00002-7)
- Mishchenko, M. I., & Yurkin, M. A. (2017). On the concept of random orientation in far-field electromagnetic scattering by nonspherical particles. *Optics Letters*, 42(3), 494–497. <https://doi.org/10.1364/OL.42.000494>
- Moersch, J. E., & Christensen, P. R. (1995). Thermal emission from particulate surfaces: A comparison of scattering models with measured spectra. *Journal of Geophysical Research*, 100(E4), 7465–7477.
- Muironen, K., Markkanen, J., Väisänen, T., Peltoniemi, J. I., & Penttilä, A. (2017). Multiple scattering in discrete random media using first-order incoherent interactions. *Radio Science*, 52, 1419–1431. <https://doi.org/10.1002/2017RS006419>
- Muironen, K., Markkanen, J., Väisänen, T., Peltoniemi, J., & Penttilä, A. (2018). Multiple scattering of light in discrete random media using incoherent interactions. *Optics Letters*, 43(4), 683–686.
- Muironen, K., Markkanen, J., Virkki, A., Penttilä, A., & Mackowski, D. (2016). *Multiple scattering by dense random media: Volume-element extinction*. Paper presented at 2016 URSI International Symposium on Electromagnetic Theory (EMTS), (pp. 751–754).
- Muironen, K., Penttilä, A., & Videen, G. (2015). Multiple scattering of light in particulate planetary media. In L. Kolokolova, J. Hough, & A. Levasseur-Regourd (Eds.), *Polarimetry of Stars and Planetary Systems* (pp. 114–129). Cambridge, UK: Cambridge University Press. <https://doi.org/10.1017/CBO9781107358249.018>
- Muñoz, O., Volten, H., Hovenier, J. W., Veihelmann, B., van der Zande, W. J., Waters, L. B. F. M., & Rose, W. I. (2004). Scattering matrices of volcanic ash particles of Mount St. Helens, Redoubt, and Mount Spurr Volcanoes. *Journal of Geophysical Research*, 109, D16201. <https://doi.org/10.1029/2004JD004684>
- Mustard, J. F., & Hays, J. E. (1997). Effects of hyperfine particles on reflectance spectra from 0.3 to 25 μm . *Icarus*, 125, 145–163.
- Ohtake, M., Matsunaga, T., Yokota, Y., Yamamoto, S., Ogawa, Y., Morota, T., et al. (2010). Deriving the absolute reflectance of lunar surface using SELENE (Kaguya) multiband imager data. *Space Science Reviews*, 154(1–4), 57–77. <https://doi.org/10.1007/s11214-010-4566-0>
- Pan, C., Rogers, A. D., & Thorpe, M. T. (2015). Quantitative compositional analysis of sedimentary materials using thermal emission spectroscopy: 2. Application to compacted fine grained mineral mixtures and assessment of applicability of partial least squares methods. *Journal of Geophysical Research: Planets*, 120, 1984–2001. <https://doi.org/10.1002/2015JE004881>
- Papike, J., Taylor, L., & Simon, S. (1991). Lunar minerals. In G. H. Heiken, D. T. Vaniman, & B. M. French (Eds.), *Lunar Source Book* (pp. 121–181). New York: Cambridge University Press.
- Pieters, C. M., Goswami, J. N., Clark, R. N., Annadurai, M., Boardman, J., Buratti, B., et al. (2009). Character and spatial distribution of OH/H₂O on the surface of the moon seen by M³ on Chandrayaan-1. *Science*, 326(5952), 568–572. <https://doi.org/10.1126/science.1178658>
- Pitman, K. M., Kolokolova, L., Verbiscer, A. J., Mackowski, D. W., & Joseph, E. C. S. (2017). Coherent backscattering effect in spectra of icy satellites and its modeling using multi-sphere T-matrix (MSTM) code for layers of particles. *Planetary and Space Science*, 149, 23–31. <https://doi.org/10.1016/j.pss.2017.08.005>
- Pitman, K. M., Wolff, M. J., & Clayton, G. C. (2005). Application of modern radiative transfer tools to model laboratory quartz emissivity. *Journal of Geophysical Research*, 110, E08003. <https://doi.org/10.1029/2005JE002428>
- Poulet, F., Bibring, J.-P., Langevin, Y., Mustard, J. F., Mangold, N., Vincendon, M., et al. (2009). Quantitative compositional analysis of martian mafic regions using the MEX/OMEGA reflectance data 1. Methodology, uncertainties and examples of application. *Icarus*, 201(1), 69–83. <https://doi.org/10.1016/j.icarus.2008.12.025>
- Poulet, F., Cuzzi, J. N., Cruikshank, D. P., Roush, T., & Dalle Ore, C. M. (2002). Comparison between the Shkuratov and Hapke scattering theories for solid planetary surfaces: Application to the surface composition of two centaurs. *Icarus*, 160(2), 313–324. <https://doi.org/10.1006/icar.2002.6970>
- Poulet, F., Mangold, N., Loizeau, D., Bibring, J.-P., Langevin, Y., Michalski, J., & Gondet, B. (2008). Abundance of minerals in the phyllosilicate-rich units on Mars. *Astronomy and Astrophysics*, 487(2), L41–L44. <https://doi.org/10.1051/0004-6361/200810150>
- Ramezan pour, B., & Mackowski, D. W. (2017). Radiative transfer equation and direct simulation prediction of reflection and absorption by particle deposits. *Journal of Quantitative Spectroscopy and Radiative Transfer*, 189, 361–368. <https://doi.org/10.1016/j.jqsrt.2016.11.028>
- Ramsey, M. S., & Christensen, P. R. (1998). Mineral abundance determination: Quantitative deconvolution of thermal emission spectra. *Journal of Geophysical Research*, 103, 577–596. <https://doi.org/10.1029/97JB02784>
- Reichardt, T. A., & Kulp, T. J. (2016). Radiative transfer modeling of surface chemical deposits. *Proceedings of SPIE*, 9840. <https://doi.org/10.1117/12.2224071>
- Rogers, A. D., & Aharonson, O. (2008). Mineralogical composition of sands in Meridiani Planum determined from Mars Exploration Rover data and comparison to orbital measurements. *Journal of Geophysical Research*, 113, E06S14. <https://doi.org/10.1029/2007JE002995>
- Rogers, A. D., Bandfield, J. L., & Christensen, P. R. (2007). Global spectral classification of Martian low albedo regions with Mars Global Surveyor Thermal Emission Spectrometer MGS TES data. *Journal of Geophysical Research*, 112, E02004. <https://doi.org/10.1029/2006JE002726>
- Rucks, M., & Glotch, T. D. (2014). *Mid IR optical constants of orthopyroxenes*. Paper presented at AGU Fall Meeting, Abstract P23B-3987.
- Salisbury, J. W. (1993). Mid-infrared spectroscopy: Laboratory data. In C. Pieters & P. Englert (Eds.), *Remote Geochemical Analysis: Elemental and Mineralogical Composition* (pp. 79–98). New York: Cambridge University Press.
- Salisbury, J. W., & Wald, A. (1992). The role of volume scattering in reducing spectral contrast of reststrahlen bands in spectra of powdered minerals. *Icarus*, 96(1), 121–128. [https://doi.org/10.1016/0019-1035\(92\)90009-V](https://doi.org/10.1016/0019-1035(92)90009-V)
- Shkuratov, Y., Starukhina, L., Hoffmann, H., & Arnold, G. (1999). A model of spectral albedo of particulate surfaces: Implications for optical properties of the moon. *Icarus*, 137(2), 235–246. <https://doi.org/10.1006/icar.1998.6035>
- Smith, M. D., Bandfield, J. L., & Christensen, P. R. (2000). Separation of atmospheric and surface spectral features in Mars Global Surveyor Thermal Emission Spectrometer (TES) spectra. *Journal of Geophysical Research*, 105, 9589–9607. <https://doi.org/10.1029/1999JE001105>
- Thorpe, M. T., Rogers, A. D., Bristow, T. F., & Pan, C. (2015). Quantitative compositional analysis of sedimentary materials using thermal emission spectroscopy: 1. Application to sedimentary rocks. *Journal of Geophysical Research: Planets*, 120, 1956–1983. <https://doi.org/10.1002/2015JE004863>
- Tishkovets, V. P. (2008). Light scattering by closely packed clusters: Shielding of particles by each other in the near field. *Journal of Quantitative Spectroscopy and Radiative Transfer*, 109(16), 2665–2672. <https://doi.org/10.1016/j.jqsrt.2008.05.008>
- Tishkovets, V. P., & Petrova, E. V. (2013a). Coherent backscattering by discrete random media composed of clusters of spherical particles. *Journal of Quantitative Spectroscopy and Radiative Transfer*, 127, 192–206. <https://doi.org/10.1016/j.jqsrt.2013.05.017>
- Tishkovets, V. P., & Petrova, E. V. (2013b). Light scattering by densely packed systems of particles: Near-field effects. In A. A. Kokhanovsky (Ed.), *Light Scattering Reviews 7: Radiative Transfer and Optical Properties of Atmosphere and Underlying Surface* (pp. 3–36). New York: Springer. https://doi.org/10.1007/978-3-642-21907-8_1

- Tishkovets, V. P., & Petrova, E. V. (2016). On applicability of the far-field approximation to the analysis of light scattering by particulate media. *Journal of Quantitative Spectroscopy and Radiative Transfer*, *182*, 24–34. <https://doi.org/10.1016/j.jqsrt.2016.05.013>
- Tishkovets, V. P., & Petrova, E. V. (2017). Reflectance model for densely packed media: Estimates of the surface properties of the high-albedo satellites of Saturn. *Solar System Research*, *51*(4), 277–293. <https://doi.org/10.1134/S0038094617040062>
- Tsang, L. (1992). Dense media radiative transfer theory for dense discrete random media with spherical particles of multiple sizes and permittivities. In A. Priou (Ed.), *Progress in Electromagnetics Research* (Vol. 6, *Dielectric Properties of Heterogeneous Materials* (pp. 181–230). New York: Elsevier Sci.
- Tsang, L., Kong, J. A., & Shin, R. (1985). *Theory of Microwave Remote Sensing*. New York: Wiley-Interscience. [https://doi.org/10.1016/0022-2836\(85\)90405-X](https://doi.org/10.1016/0022-2836(85)90405-X)
- van de Hulst, H. C. (1957). *Light scattering by small particles*. New York: John Wiley.
- Videen, G., & Muinonen, K. (2015). Light-scattering evolution from particles to regolith. *Journal of Quantitative Spectroscopy and Radiative Transfer*, *150*, 87–94. <https://doi.org/10.1016/j.jqsrt.2014.05.019>
- Vincent, R. K., & Hunt, G. R. (1968). Infrared reflectance from mat surfaces. *Applied Optics*, *7*(1), 53–59. <https://doi.org/10.1364/AO.7.000053>
- Wald, A. E. (1994). Modeling thermal infrared (2–14 μm) reflectance spectra of frost and snow. *Journal of Geophysical Research*, *99*, 24,241–24,250. <https://doi.org/10.1029/94JB01560>
- Wald, A. E., & Salisbury, J. W. (1995). Thermal infrared directional emissivity of powdered quartz. *Journal of Geophysical Research*, *100*, 24,665–24,675. <https://doi.org/10.1029/95JB02400>
- Wiscombe, W. J., & Warren, S. G. (1980). A model for the spectral albedo of snow. I: Pure snow. *Journal of Atmospheric Science*, *37*(12), 2712–2733. [https://doi.org/10.1175/1520-0469\(1980\)037%3C2712:AMFTSA%3E2.0.CO;2](https://doi.org/10.1175/1520-0469(1980)037%3C2712:AMFTSA%3E2.0.CO;2)
- Wolff, M. J., & Clancy, R. T. (2003). Constraints on the size of Martian aerosols from Thermal Emission Spectrometer observations. *Journal of Geophysical Research*, *108*(E9), 5097. <https://doi.org/10.1029/2003JE002057>
- Wolff, M. J., Smith, M. D., Clancy, R. T., Arvidson, R., Kahre, M., Seelos, F. IV, et al. (2009). Wavelength dependence of dust aerosol single scattering albedo as observed by the Compact Reconnaissance Imaging Spectrometer. *Journal of Geophysical Research*, *114*, E00D04. <https://doi.org/10.1029/2009JE003350>
- Wolff, M. J., Smith, M. D., Clancy, R. T., Spanovich, N., Whitney, B. A., Lemmon, M. T., et al. (2006). Constraints on dust aerosols from the Mars Exploration Rovers using MGS overflights and Mini-TES. *Journal of Geophysical Research*, *111*, E12S17. <https://doi.org/10.1029/2006JE002786>
- Xiong, C., & Shi, J. (2014). Simulating polarized light scattering in terrestrial snow based on bicontinuous random medium and Monte Carlo ray tracing. *Journal of Quantitative Spectroscopy and Radiative Transfer*, *133*, 177–189. <https://doi.org/10.1016/j.jqsrt.2013.07.026>
- Xiong, C., Shi, J., Ji, D., Wang, T., Xu, Y., & Zhao, T. (2015). A new hybrid snow light scattering model based on geometric optics theory and vector radiative transfer theory. *IEEE Transactions on Geoscience and Remote Sensing*, *105*(9), 4862–4875. <https://doi.org/10.1109/TGRS.2015.2411592>
- Zur, L. M., Tsang, L., & Winebrenner, D. P. (1996). Scattering properties of dense media from Monte Carlo simulations with application to active remote sensing of snow. *Radio Science*, *31*, 803–819. <https://doi.org/10.1029/96RS00939>